Effects of Bending and Stretching on Hybrid Organic- Inorganic Trihalide Perovskite Solar Cells

Musibau Francis Jimoh

Professor Wiston W. Soboyejo

A Thesis Submitted for

the award of the Degree of Master of Science

Department of Materials Science & Engineering

African University of Science and Technology, Abuja

December, 2014

Abstract

In the recent decade, hybrid organic- inorganic trihalide perovskite solar cells have attracted significant interest from the scientific community due to their unique optoelectrical properties, ease and low cost of fabrication. Extensive research has been carried out to understand the electrical and optical properties of this novel material with a view to boosting the efficiency of the system. However, not much has been done to understand the mechanical properties of the system. The potential brittleness which predisposes the system to crack has not been addressed. In addition, issues with regards to the response of the cell to stretching and bending have not been investigated. In this research work, lead-based and tin-based perovskite solar cells were modeled and subjected to bending and stretching forces using ABAQUS^{TM} finite element analysis software. Preliminary analysis showed that PET is a more suitable substrate for bending applications while PDMS is more compliant for stretching purposes. Contour plots obtained showed that the relatively high modulus of elasticity and layer thickness of TiO_2 nanocrystals reduces the mechanical performance of the solar cells where flexibility is desirable. High stress levels were observed on the aluminium contact layer of the structures; this is due to the huge difference in elasticity between aluminium and the organic and organic-inorganic materials. Although some immediate conclusion can be made from the results presented, implications of some of the results obtained are still unclear. It is therefore recommended that experimental work be undertaken to verify the result obtained from the simulations done. Further investigation and experimentation into cracks and failure mechanisms not covered in this research is strongly recommended in future work.

Acknowledgements

Inestimable praise, thanks and adoration goes to God Almighty, in whom all things consist, for His infinite mercies, loving kindness and divine favour towards me. All I am and will ever be is you Lord.

Special appreciation goes to my supervisor, Professor Wole Soboyejo for his unflinching understanding, support and guidance which culminated in the success of this research. He has imprinted in me scholarship tempered with character.

I also express deep appreciation to Dr Omololu Akinojo and Prof. Zebaze-Kana. Your insights, kind words and counsels made the difference. Worthy of mention are Messers Joseph Asare, Chukwuemeka Ani and Kehinde Oyewole for their technical assistance and encouragements.

Special thanks to my Sponsor, African Capacity Building Fund (ACBF). Thank you for offering me your wings to fly.

Innumerable thanks go to my Mothers Mrs Bisi Ayodele and Mrs Rachael Alao for literarily putting their lives on hold that I may live. May God satisfy you with peace, long-life and sound health and fill your years with love.

I am forever indebted to my Life Coach Daddy Jerry Christon, and my Father/ Mentor Colonel Babatunde Babalola (Rtd), for their love, counsels and encouragements, moral and financial support. May God's love and joy never cease in your lives.

Profound appreciation goes to my true family; Miss: Temitayo Ayodele, Olayemi Ayodele, Modupe Christiana Alao, Messers: Solomon Ayodele, Saheed Agboola Suleiman, Opeyemi Sunday Oyebode, Mrs Hope Jumie Landop, Mr Israel Adebayo Oyebamiji & family, Mr Kazeem Amuzat & family.

I am particularly grateful to Mummy Virgie Ofordile, Mummy Fidelia Ogbuzuo (Our Family Fellowship) Prof and Mrs Olusola Oni (Family Worship Centre, Abuja), Prof Olusegun O. Adewoye, Dr Philip Enegela, Miss Bolade Igbagbo, for their moral, financial and spiritual support. May the glory of God continue to manifest in your lives and endeavours.

To all of my course mates, friend and well-wishers you are greatly appreciated. Hope to see you all among the 'stars,' illuminating our universe. God bless you.

Table of Contents

List of Figures

List of Tables

Appendix A

1. CHAPTER ONE: INTRODUCTION

1.0 Background

Rapid improvement in man's living standard and daily living conveniences such as the use of electric bulb, telephone, air conditioners, street lighting systems, transportation, and powering of machineries in industries, are largely due to the availability of energy sources which act as the drivers of these systems.

However, in a bid to generate the required energy needed to operate these systems, various energy sources such as fossil fuels, bio fuels, wind, hydro, nuclear and solar have been exploited each of which has its peculiar advantages and drawbacks. Some of these includes: water and atmospheric pollution, high cost of maintenance, competition for food, potential dangers of leakage and waste disposal (in nuclear plants) (Win, 2006).

Solar energy seems more promising among all the aforementioned existing sources of energy. Energy from the sun is enormous, clean, cheap and eco-friendly (i.e. carbon free). It is sustainable and indefinitely renewable since the sun which is its source and central to the sustenance of life is in theory inexhaustible in several millions of years (IEA, 2011; Tsao, et al., 2006). In addition, solar panel, a photovoltaic device used for photo-conversion can produce electricity at dimension of few millimeters with little or no maintenance needed once installed. They produce electricity silently and are an excellent choice when avoiding noise pollution.

In an effort to harness the abundant energy of the sun for electricity, several photovoltaic systems have been fabricated by researchers. These systems are varied in power conversion efficiency, which depend on the fabrication technique and materials used. Common photovoltaic systems are the silicon based solar cells, organic solar cells, dye sensitized solar cells, and carbon based solar cells (which are championed by graphene). However, the fabrication of these electronics requires ultra-pure and expensive materials, high-tech processing, with environmental challenges and other attendant issues such as stability, efficiency and scalability.

In the recent decade, perovskite-based electronics have attracted significant interest from the scientific community. Perovskite is a novel hybrid organic-inorganic trihalide photoactive materials that have been used to improve the performance of solar cells. This material combines the excellent properties of both organic and inorganic solar cells, and have unique optical (large absorption coefficient) (Lang *et al.,* 2014) and electrical properties (high carrier mobility and diffusion length) (Liu *et al.,* 2013). They can easily be processed from solution at

low temperature in large scale, using cheap materials. They also offers the opportunity of high incident photon to power conversion efficiency (IPCE) if properly tuned (Liu, Johnston & Snaith, 2013; Burschka, Pellet, Moon, *et al.*, 2013; Qin, Tanaka, Ito, *et al.*, 2014).

With an increasing demand for electronics that are light weight, flexible and can easily be manufactured using printing or lamination technology, these perovskite-based electronics can be made stretchable and bendable on compliant substrate and adapted for solar cell applications.

During service however, stretching and bending of electronic materials can lead to buckling, a wavy-like deformation which could further lead to delamination at the interface of the materials. Winkling, cracks, creep and fracture are common mechanical failures associated with stretching and bending of wearable electronic structure.

Hence, an understanding of how perovskite-based solar cells respond to stretching and bending, how this affects the interfacial failure between the layers of the cell and the distribution of stress in the layers will help in the integration of this cheap and increasingly efficient material into applications such as e-textiles, solar bags, roof of buildings and even modern flexible electronics.

1.1 Unresolved Issues

A lot of research has been done to understand the electrical and optical properties of perovskite based solar cells. The mechanisms of light harvesting/absorption, charge separation and transport with a view to boosting the efficiency of the system has also enjoyed wide coverage. Increasingly, researches are also currently being carried out to improve the architecture, processing techniques and further reduce the cost of this solar cell.

However, not much has been done to understand the mechanical properties of the system. The potential brittleness which predisposes the system to crack has not been addressed. Also, issues with regards to the response of the cell to stretching and bending needs to be investigated. The effect of bending or stretching on the efficiency of the system as well as the strain limit in bending, stretching or torsion has not been researched. Literatures on prediction of the failure mechanism of the systems are also not readily available. This may be attributed to the limited research in that field since the material is relatively new.

Even though efforts have been made and are still being made to address the potential toxicity of lead by replacing it with tin, the response of each of these systems as well as their cell to bending and stretching stresses has also not been fully considered and this could play a role as to which should be focused on.

1.2 Aim and Objectives of the Thesis

The aim of this research work is to study the response of lead-based and tin-based perovskite solar cells to bending and stretching forces with a view to designing a robust stretchable and bendable perovskite solar cell.

The objectives are to:

i. observe stress distribution through the perovskite layer and a model perovskite-based cell,

ii. how crack propagates through the layers and to

iii. predict their failure mechanisms.

1.3 Scope of the Thesis

This research work covers the collection of key mechanical properties of layered lead and tin based perovskite solar cells from available literature. The failure mechanisms of the layered devices are then studied using ABAQUS^{TM} software. The implications of the results obtained were discussed and recommendations made for future design of stretchable and bendable perovskite solar cells.

1.4 Thesis Layout

Chapter one gives a background of energy and the importance of energy to man's socio-economic activities. It gives an overview of energy sources, the efforts made as well as the limitations of each of the energy source.

Chapter two presents a literature survey of the world's energy need as it relates to her present and projected population. It provides an insight into the energy challenges of Africa and it consequences on her socioeconomic life. A cursory view of other types of solar cells as well as

perovskite solar cells, and a closer view of the work done on perovskite-based solar cells was presented.

In chapter three, numerical and computational models of bending and stretching were presented and the results obtained were presented and discussed in chapter four. Conclusions were drawn in chapter five and recommendations for future work made.

2 Chapter Two: Literature Review

2.1 Global and African Energy Challenge

The world population as at 2013 was approximately 7.2 billion, and this has been projected to peak at 9.6 billion by 2050 (http://esa.un.org/). The implication of this projection is that the world's energy consumption would increase from its value of 13.5TW in 2001 to 27.6 TW by 2050 (http://www.sandia.gov). Africa, with a population of approximately 1.1 billion in 2013 is expected to peak at 2.4 billion (representing 19% of the world's population) by 2050. Out of the 1.1 billion of Africa's population at the moment, 587 million does not have access to electricity, 585 million of which are in sub Saharan Africa [http://www.unesco.org/].

To a larger degree, developed nations have been able to meet their present energy demands considerably by combining various energy sources like fossil fuel, and nuclear and are investing greatly in the research and development of alternative renewable energy sources such as wind power, biomass, geothermal, and solar for their projected growing population. African however hasn't done much to meet her present energy need and probably have no plans for her future population. The implication of this is that not only will 19% of the world's population have limited access to power; they will also remain underdeveloped and poor since power is one of the fundamental requirements for the development of any economy.

With an estimated 175,000 TW of solar energy reaching the earth annually, about 35% strikes the African continent. It is therefore imperative that Africa given her rich supply of solar energy harness this "free", clean and cheap gift of nature to meet her growing population and energy demands for improved economic activities and standard of living. This chapter examines prior research on different photovoltaic systems, efforts made to increase their flexibility as well as their degradation mechanisms.

2.2 Photovolatics

Photovoltaic devices are based on the concept of charge separation at an interface of two materials of different conduction mechanism when light is incident on it. Various technologies have been developed to harness sunlight each of which has it peculiar materials, strengths and weaknesses.

2.2.1 Inorganic Solar Cells

Inorganic solar cells are the most commonly used photovoltaic. This type of solar cell is championed by crystalline silicon (c-Si) whose production increase has been put at 35% each year (Mcgehee 2009), and accounts for 83% of all the commercially available solar cell in 2011 (Saga, 2010). Cadmium Telluride, Copper Indium (di)Selenide (CIGS), Gallium Arsenide GaAs are other types of thin film inorganic photovoltaic cells and they all account for the remaining 17%.

Silicon based systems delivers current when n-doped and p-doped silicon are arranged together in p-n junction either in series or parallel. The incident solar radiation produces electrons in the p-type and holes in the n-type, and a lower potential energy barrier results causing current to flow and hence establish an external potential. The prominent position of silicon-based solar cells is due to its safety and relative abundance on earth.

One limitation of c-Si is it indirect bandgap which gives it a low optical absorption coefficient hence wafers need to have thickness greater than 200 μm for optimum light harvest. Other drawbacks are poor flexibility and stretchability, as well as the need for ultra-pure fabrication environment which makes it high-tech and expensive. Silicon-based PV technologies have also matured as its efficiency is approaching the predicted theoretical efficiency of 30% hence research on it is slowing down.

GaAs, GaSb, CIGS and InP, have been reported to have direct energy bandgaps, relatively high optical absorption coefficients compared to C-Si, and fairly reasonable values of carrier mobilities and lifetimes. Competitive efficiencies have been reported for photovoltaic cells made using this class of inorganic materials (Bube, 1998). High cost of fabrication, bulkiness, significant reduction in efficiency due to defects in crystals and weak mechanical robustness which causes easy cleavage has made these materials unsuitable as large scale commercial replacement for silicon (Miles *et al.,* 2007). This has therefore necessitated a less expensive material with promising efficiency for PV application and mechanically more forgiving.

2.2.2 Organic Based Solar Cells

The structure of a typical OPV consists of a photoactive material sandwiched between two charge transporting materials of different work functions. The photoactive layer absorbs sunlight to generate excitons, from which electrons are excited from the valence band to the conduction band. Concentration gradient encourages the excitons to diffuse to the interfaces of the

donor/acceptor layers and dissociate into positive charge carriers (free holes) and negative charge carriers (electrons). The movement of these carriers to the respective electrodes generates photocurrents (Arkhipov & Bässle, 2004).

Interesting organic materials such as polyphenyl vinylene (PPV), polythiophene (PT), poly (3-hexylthiophene) (P3HT), ([6,6]-phenyl C61-butyric acid methylester) (PCBM) have enjoyed significant attention from scientist for photovoltaic applications. OPV has an advantage of flexibility, lower material and manufacturing cost over inorganics. To improve efficiencies and flexibility, different architectures of OPVs such as single junction, bilayer, bulk-heterojuction (Yu et al 1995), graded junction and inverted device structures (Kaltenbrunner, White, Głowacki, *et al.*, 2012) have been reported. Optimisation of mechanical stability and improved film morphologies are also indispensable to wide scale wearable organic solar cell fabrication.

2.2.3 Dye Sensitized Solar Cell

Unlike in conventional C-Si PV systems where light absorption and charge carrier transportation is performed by a single material, these functions are separated in dye sensitized solar cells (DSSC). Light harvest is done by a sensitizer attached to the surface of a semiconductor with wide bandgap, while charge separation occurs at the interface via photo-induced electron injection from the dye into the conduction band of the solid.

Carriers are transported in the conduction band of the semiconductor to the charge collector. The dye is afterward restored to the neutral state by electron donation from the electrolyte usually an organic solvent containing redox system, such as the iodide/triiodide couple (Grätzel, 2003). The use of sensitizers with a broad absorption band in conjunction with oxide films of nanocrystalline morphology has been reported to enhance the harvest of a large fraction of sunlight (Campbell et al., 2007; Hardin *et al.,* 2012).

Some of the advantages of DSSC include cheap materials needed for fabrication, relatively high efficiency, elimination of charge recombination since no hole is generated when electron is injected into the nanostructured metal oxide (rather, another electron is added). This enables DSSC to work even under diffuse light unlike other PV technologies (Hug *et al.,* 2014). Solid state DSSCs are mechanical robust and the efficiency of DSSC generally is limited to the amount of photon the dye can absorb.

Although it boasts of some of the best efficiency published so far for solution- processed PV devices, one of the major limitation of DSSC is their high temperature sensitivity, which makes them unusable at relatively low temperatures as electrons freezes or the liquid electrolytes expands at high temperatures thereby posing the challenge of sealing the cell (Shauddin, 2013). In addition to this, other drawbacks includes the cumbersome nature of the cell (hence cannot be really made flexible), potential long time instability as well as the evaporation, potential leakage and corrosion characteristic of liquid-based DSSC (Docampo, Guldin, Leijtens, *et al.*, 2014; Hardin, Snaith & McGehee, 2012; Grätzel, 2003).

2.2.4 Carbon Based Solar Cells

Carbon is highly attractive for possible application in photovoltaic solar cells. It is a highly stable, cheap and nontoxic material, which can be obtained from precursors that are sufficiently available in nature. Ramuz *et al.,* (2012) reported an all-carbon solar cell where the photoactive layer and transport layers are all carbon based. An efficiency of 0.46% and 0.13% was reported under AM 1.5 and NIR illumination respectively. The low yield was attributed to high leakage, roughness and contamination issues in the films type.

Jeong *et al.,* (2011) also fabricated an all-carbon nanotube based flexible PV. The system is composed of anode and cathode electrodes composed of carbon nanotubes and a carbon nanotube/ tetraethylorthosilicate hybrid film produced by doping technique. Their result basically illustrated the advantages of using a carbon-based material by demonstrating its high flexibility and environmental stability when compared to devices composed of other materials.

Recently, fullerenes have also been incorporated in organic photovoltaics (OPVs) (Khlyabich *et al.,* 2013; Lai *et al.,* 2014; Sariciftci, 1999). Fullerene derivatives, like [6,6]- phenyl-C_{61}-butyric acid methyl ester ($PC_{60}BM$), are the most commonly used acceptor material in OPVs due to their high electron affinity (Scharber, Mühlbacher, Koppe, *et al.*, 2006), although there has been a demonstration of using C_{60} as the primary active element in an OPV (Chen *et al.,* 2011). Graphene and grapheme oxide (GO) have predominately been used in PVs as electrodes and hole transport layers, respectively (Hsu, Lin, Huang, *et al.*, 2012).

Although carbon based solar cells boosts of lower cost and mechanical robustness, it generally has lower efficiency. There is thus a need for better, more efficient, stable solar cells that are easier to process and mechanically robust.

2.2.5 Perovskite Solar Cells

Following the pioneering work of Gratzel and Brian, on dye sensitized solar cell in 1991, Miyasaka et al., (2009) published a seminal paper on new solar cells which are sensitized by organo-metal halides. Newly discovered perovskite solar cells belongs to a class of hybrid organic-inorganic solid state solar cells and combines the unique properties of both organic and inorganic solar cell.

Earlier works by researchers have shown that this material possess excellent optical and charge carrying abilities. This class of materials has shown attractive properties like superconductivity, ferroelectricity as well as excellent structural, elastic and magnetic properties (Jarlborg, 1998; Ondrejkovic et al, 2013; Zhang et al, 2001)

2.2.5.1 Structure and Properties of Photoactive Perovskite Material

Perovskite is a general name for materials with the structure ABX_3 where *A* and *B* can be any suitable organic or inorganic cations, and X can be oxygen or halogens. In the recent decade, hybrid organic-inorganic trihalide perovskite (HOITP) material, $CH_3NH_3BX_3$ (B= Pb, Sn; X=Cl, Br, I) has gained wide use for electronic applications such as solar cells (Choi *et al.,* 2014; Docampo *et al.,* 2013; Heo *et al.,* 2013; Miyasaka *et al.,* 2009; Lee *et al.,* 2012), light emitting diode (Tan *et al.*, 2014), laser generation (Xing *et al.*, 2014; Deschler *et al.*, 2014) and a variety of electromechanical devices. They have been reported to exist in three phases: psuedocubic at high temperature, tetragonal at medium temperature and orthorhombic at low temperature (Feng, 2014).

They have however attracted widespread attention for photovoltaic application largely due to their unique optical (large absorption coefficient) and electrical properties (high carrier mobility and diffusion length) (Brivio *et al.,* 2013; Lang, Yang *et al.,* 2014; Qin *et al.,* 2014), ease of processing from solution at low temperature even at large scale (Xing *et al.*, 2014; Docampo *et al.*, 2013; You *et al.*, 2014), and stability in air (Kim *et al.,* 2014; Seetharaman *et al.,* 2014; Smith *et al.,* 2014). In addition, the precursor materials are cheap and they offer the opportunity of high incident photon to power conversion efficiency (IPCE) if properly tuned. The generation of charges inside the bulk material as well as the separation of the function of light absorption and charge carrier transport reduces energy loss and charge recombination (Edri *et al.*, 2014).

2.2.5.2 Architectures of Perovskite-Based Solar Cells

Following from the work of Gratzel and Miyasaka, earlier architectures of the perovskite-based solar cells were similar to DSSC where the light absorber is deposited on the nanostructured mesoporous metal oxide (Choi *et al.*, 2014; Kojima *et al.*, 2009; Lee *et al.*, 2012). This sensitized-type architecture was initially thought to be responsible for the increase in efficiency of the cell. Recent research however shows that simple planar architecture where the perovskite is sandwiched/ interposed between the densely packed TiO_2 layer and a hole conducting layer can not only give comparable high efficiency but eliminate the need for high temperature sintering and also improves the ease of manufacturing the device on flexible substrate (Docampo *et al.*, 2013; Liu & Kelly, 2013; You *et al.*, 2014; Kim *et al.*, 2014). Also, cell designed with hetero-junction architecture has been reported to give a better efficiency than the single junction (Kim *et al.,* 2012; Lee *et al.,* 2012). Heo et al., (2013) reported that in planar architecture, perovskite due to it ambipolar nature can function as a p or n-type conductor.

Variation has been observed in the morphology of the different perovskite solar cell architectures produced using traditional method of deposition. This has been been attributed to the uncontrolled precipitation of the perovskite in the mesoporous TiO_2. Sequential method of depositing the perovskite precursor materials into the pores was proposed by Burschka *et al.*, (2013). The lead iodide was deposited first into the pores of mp-TiO_2 and sintered first after which it is dipped in methyl iodide for the formation of the perovskite structure. This method was reported to give a stable cell with a reproducible high efficiency.

2.3 Stretchable and Bendable Solar Cells

Great amount of research efforts have been invested towards manufacturing flexible and wearable solar cells. Conditions such as improved adhesion between thin film layer(s) and flexible substrate, fabrication route and dimensional stability (creep control) are required for the fabrication of flexible and stretchable solar cells.

2.3.1 Flexible and Stretchable Conventional Photovoltaic Technologies

Common failures of wearable solar cells reported in literature include but not limited to delamination, flaking, buckling, cracks and fracture. These have been attributed to factors like microstructure of materials, impurities in materials and residual thermal stresses during fabrication. Other causes of failure often cited are surface roughness of materials, method of

film deposition, as well as the mismatch of glass transition temperature and coefficient of expansivity of substrates and film layers.

Lipomi and coworkers (2011) investigated the stretchability of organic solar cells fabricated directly on pre-stretched PDMS of thickness ranges of 200-500 μm. They reported a reversible tensile strain of about 27%. Mechanical stability of the cells was improved upon by employing liquid metal as back contact. Lee *et al.,* (2011) reported an array of flexible and stretchable GaAs microcells supported on PDMS. They presented tensile strain of 20% with a radius of curvature of 1.5 mm. Kaltenbrunner and coworkers (2012) in their study of ultrathin, light, flexible and compliant OPV devices on PET published result of cells with a PCE of 4.2%. The cells are highly flexible with reversible tensile strains of over 300% when supported on elastomeric material.

Experimental characterization of microwrinkling, microbuckling and adhesion between layers of OPVs, OLEDs and other hybrid photovoltaic using Atomic force microscopy (AFM) (Tong *et al.,* 2009) and Scanning Electron Microscopy (Kaltenbrunner, White, Głowacki, *et al.*, 2012) have been widely reported. This has provided insights into the relationship between mechanical degradation and cell microstructure.

2.3.2 Flexible and Stretchable Perovskite-Based Solar Cells

Limited literature exists on the fabrication and characterize of flexible perovskite-based solar cells. Notable efforts however are the works of Docampo *et al.*, (2013), Liu and coworkers, (2013), You *et al.*, (2014), Kim *et al.*, (2014), Malinkiewicz *et al.*, (2013), Liu & Kelly (2013) and Conings *et al.*, (2014).

In these works, flexibility is achieved using different processing techniques, charge transporting materials and cell architecture. One of the ways through which this has been achieved is incorporating organic charge transport materials and using TiO_2 nanoparticle dispersion instead of compact TiO_2 layer that requires a high temperature.

Kim and coworkers (2014) reported an efficiency of 12.2% for a mono layer of compact TiO_2 perovskite solar cell deposited on polyethylene napthalate. They emphasized the novelty of the high efficiency and bendability obtained and noted that low temperature deposition process of the TiO_2 layer is central to obtaining such result. Novel methods of depositing the TiO_2 for roll - roll fabrication of wearable perovskite solar cell include ultra-sonic spray-coating (Barrows *et al.,* 2014), plasma enhanced atomic layer deposition (Kim *et al.*, 2014) and blade-coating (Cho, *et al.*, 2014).

Qiu and coworkers reported a bending for 50 cycles on perovskite material integrated on flexible fibre with no obvious damage on the efficiency of the cell.

Despite the unique properties and numerous advantages of photoactive perovskite, there are some concerns about this new class of material. The highest efficiency boasted so far is obtained from the lead-based perovskite, but the manufacturing, operation and disposal of this lead-containing cell could be toxic to the environment (Green *et al.,* 2014). It has also been shown that the perovskite is unstable and rapidly degrades under ultraviolet light (Leijtens *et al.*, 2013).

To address the toxicity obstacle of perovskite cells, a number of scientist have made efforts to replace lead with tin (Hao *et al.*, 2014; Stoumpos *et al.*, 2013; Noel *et al.*, 2014; Kumar *et al.*, 2014). This effort has produced a modest efficient less than 7% with ongoing research effort to improve it. The challenge to this tin-based perovskite is the instability of Sn^{2+} in air as it oxidizes to sn^{4+} breaking down the perovskite structure with the formation of tin oxide and methylammonium iodide. An explanation for the instability has been alluded to an established fact that the stability of the 2+ oxidation state for group 14 decreases down the group (Noel *et al.*, 2014).

3 Chapter Three: Research Methodology

3.1 Overview

This chapter describes the approach employed for the determination of the effects of bending and stretching on planar tin and lead based perovskite solar cell architecture. First analytical models of bending and stretching were discussed. This was then followed by the presentation of relevant parameters required for computational modeling of the cells. Presented next were the steps/procedure involved in finite element simulation of the cells. The concluding section described in detail the process used in the validation of the models designed.

3.2 Analytical Modeling

3.2.1 Bending: Three Point Bend Test Model

In this research, the three point bend test is used because it is easy to prepare, test and analyse. Idealising the cell as a beam of length *L*, resting on two rollers support and subjected to a concentrated load *P* at its centre. For small deformation, a bending moment applied to a solid body with parallel boundary surfaces initially unconstrained will cause the structure to bend until equilibrium is established with the applied moment. Under symmetry idealisation, these surfaces will remain parallel and present a constant curvature normal to them as shown in figure (3.1). During bending, one of the surfaces undergoes compression while the other experiences tension (depending on the direction in which the bending moment is applied). At the bending axis, no strain is experienced, and the surface remains neutral through the bending.

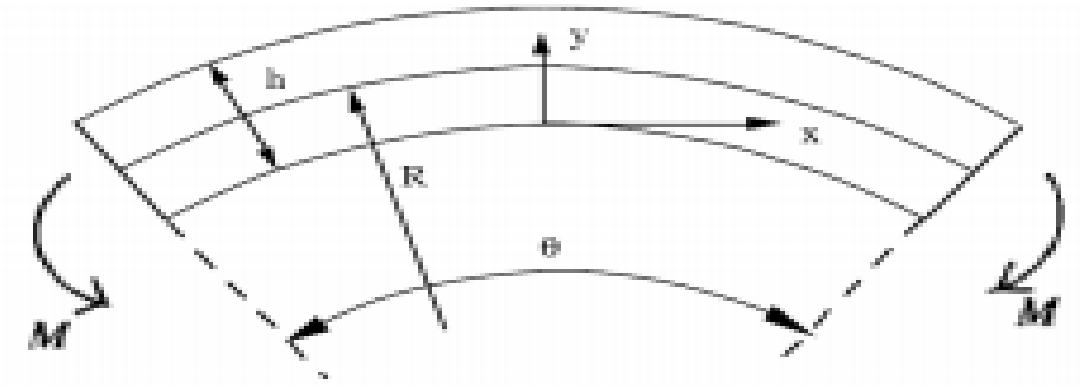

Figure 3.1: Bending moment applied to a solid body

3.2.1.1 Bending Strain

Strain is the linear variation of a dimension relatively to an initial value. Under small deformation (as earlier assumed), engineering strain (3.1) and true strain (3.2) describes the effective strain in the material (3.3).

$$\boldsymbol{\varepsilon_E = \frac{l - l_0}{l_0}} \tag{3.1}$$

$$\boldsymbol{\varepsilon_T = \int_{l_0}^{l} \frac{\delta l}{l} = ln\left(\frac{l}{l_0}\right)} \tag{3.2}$$

$$\boldsymbol{\varepsilon_T = ln(1 + \varepsilon_E)} \tag{3.3}$$

From Figure 3.1, the dimension of the bending axis is given by Rθ, where R is the radius of curvature and θ is the bending angle. The relationship between the two strains can therefore be expressed as:

$$\boldsymbol{\varepsilon_E = \frac{l - l_0}{l_0} = \frac{[R + (y - h_b)]\theta - R\theta}{R\theta} \leftrightarrow \frac{y - h_b}{R}} \tag{3.4}$$

3.2.1.2 Bending Moment and Stress Distribution

As shown in figure (3.2), a bending moment applied to a rigid body produces a linear distribution of stress in the body. This is defined along the axis of bending (h_b), by equation (3.5) in a 2-dimensional system.

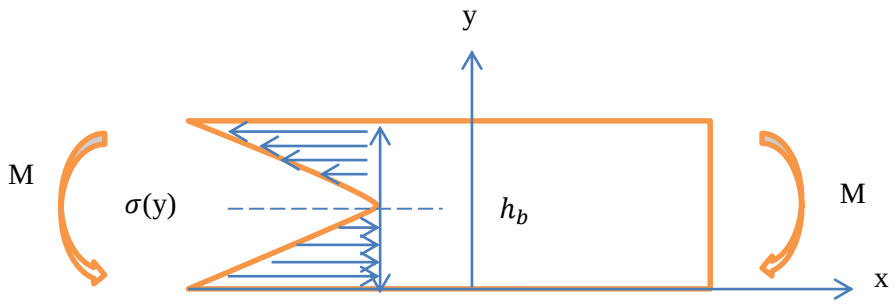

Figure 3.2: Stress distribution in a rigid body due to bending moment

$$M = \int \sigma_x (y - h_b) dy \quad (3.5)$$

3.2.1.3 Flexural Stress, Strain and Modulus

Using the bending stress equation:

$$\boldsymbol{\sigma = \frac{M_z y}{I_z}} \quad (3.6)$$

Inserting the value of the maximum moment, $M_z = \frac{PL}{4}$, the distance from the minor axis, $y = \frac{h}{2}$ and the area moment of inertia about z-axis $I_z = -\frac{bh^3}{12}$ into the bending stress equation gives the flexural stress:

$$\sigma_f = \frac{3PL}{2bh^2} \quad (3.7)$$

flexural strain:

$$\varepsilon_f = \frac{6Dd}{L^2} \quad (3.8)$$

and flexural modulus:

$$E_f = \frac{L^3 m}{4bd^3} \quad (3.9)$$

Where P is the load at a point on the load deflection curve, b is the width, d is the depth of the beam, D is the maximum deflection of the beam and L is the support span of the beam, m is the gradient of the initial straight line of the load deflection curve and E_f is the flexural modulus.

3.2.1.4 Bending Stiffness and Radius of Curvature

The bending stiffness is given by:

$$\boldsymbol{K_y = \frac{F}{\delta}} \quad (3.10)$$

If the distance from the central line to the surface of the substrate is

$$\boldsymbol{y = \frac{w}{2}} \quad (3.11)$$

Then the strain becomes;

$$\boldsymbol{\varepsilon = \frac{y}{R}} \quad (3.12)$$

Thus

$$\boldsymbol{\sigma = E\varepsilon = \frac{Ey}{R}} \tag{3.13}$$

The radius of curvature can be estimated from equation (3.13)

$$\boldsymbol{R = \frac{Ey}{\sigma}} \tag{3.14}$$

3.2.2 Stretching

Typical of thin films on flexible substrates, cracking in the metal layer as well as the photoactive perovskite materials are potential failure layers when a cell is stretched. Other types of failures such as slipping or delamination can also exist at higher film thicknesses.

As demonstrated by Akogwu *et al.,* (2010), and Oyewole (2011), applying a composite treatment to the system, the deformation of the stretchable solar cell is modeled by designating the thicknesses of the substrate (PDMS), PEDOT:PSS, Perovskite, P3HT:PCBM, TiO_2 and Al layers as t_s, t_1, t_2, t_3, t_4, t_5. Since the widths of the layers are the same, the total force of the composite is calculated thus:

$$\boldsymbol{F_C = F_s + F_1 + F_2 + F_3 + F_4 + F_5} \tag{3.15}$$

Since $F = \sigma \times A$, and given that $A_i = w \times t_i$ where $i = s, 1, 2, 3, 4, 5$

The force on each of the layers can be calculated as:

$$\boldsymbol{F_s = \sigma_s \times w \times t_s} \tag{3.16}$$

$$\boldsymbol{F_1 = \sigma_1 \times w \times t_1} \tag{3.17}$$

$$\boldsymbol{F_2 = \sigma_2 \times w \times t_2} \tag{3.18}$$

$$\boldsymbol{F_3 = \sigma_3 \times w \times t_3} \tag{3.19}$$

$$\boldsymbol{F_4 = \sigma_4 \times w \times t_4} \tag{3.20}$$

$$\boldsymbol{F_5 = \sigma_5 \times w \times t_5} \tag{3.21}$$

$$\boldsymbol{F_C = \sigma_s wt_s + \sigma_1 wt_1 + \sigma_2 wt_2 + \sigma_3 wt_3 + \sigma_4 wt_4 + \sigma_5 wt_5} \tag{3.22}$$

Expressing it as composite Area, A_c, composite stress σ_c, composite thickness t_c,

$$\boldsymbol{F_c = \sigma_c \times A_c = \sigma_c wt_c} \tag{3.23}$$

$\sigma_c wt_c = \sigma_s wt_s + \sigma_1 wt_1 + \sigma_2 wt_2 + \sigma_3 wt_3 + \sigma_4 wt_4 + \sigma_5 wt_5$

$$\boldsymbol{\sigma_c = \frac{1}{t_c}(\sigma_s t_s + \sigma_1 t_1 + \sigma_2 t_2 + \sigma_3 t_3 + \sigma_4 t_4 + \sigma_5 t_5)} \quad (3.24)$$

Since each layer has different Young's modulus, the stresses and strains in the layers is given by:

$$\boldsymbol{\sigma_i = E_i \varepsilon_i} \quad (3.25)$$

Thus

$\sigma_c = \frac{1}{t_c}(E_s \varepsilon_s t_s + E_1 \varepsilon_1 t_1 + E_2 \varepsilon_2 t_2 + E_3 \varepsilon_3 t_3 + E_4 \varepsilon_4 t_4 + E_5 \varepsilon_5 t_5)$

$$\boldsymbol{\sigma_c = \frac{1}{t_c}\left(E_s \varepsilon_s t_s + \sum_{i=1}^{N} E_i \varepsilon_i t_i\right), N = 5} \quad (3.26)$$

3.2.3 Crack Modeling

Considering a crack growing through the composite perovskite solar cell, when an applied force F_c not sufficient to damage the substrate is applied in fracture mode I, the stress concentration which describes the system is given as

$$\boldsymbol{K_I = f\sigma\sqrt{\pi a}} \quad (3.27)$$

Where a is the crack length, f is a non-dimensional geometrical function, σ is the applied stress and K_I is the stress concentration factor.

The crack energy release rate is given by

$$\boldsymbol{G = \frac{K_I^2}{E'}} \quad (3.28)$$

For plane strain condition, $\boldsymbol{E' = \frac{E}{(1-\nu^2)}}$ (3.29)

Since energy release is scalar, applying a composite treatment for mixed loading, (crack modes I, II and III) gives:

$\boldsymbol{G = G_I + G_{II} + G_{III} = \frac{K_I^2 + K_{II}^2 + (1+\nu)K_{II}^2}{E'}}$ (Soboyejo, 2003) (3.30)

3.3 Material Properties

Materials properties used for modeling were obtained from published works and duly referenced. The thicknesses of each layer are typical values reported for optimised cells in the literature.

Table 3.1: Materials properties

Material	Young's Modulus (GPa)	Poisson Ratio	Thickness (nm)	References
PDMS	0.003	0.5	1400	Lipomi *et al.,* (2012)
PET	4	0.3	1400	Y. Lee & Lee, (2014)**,** Kaltenbrunner et al., (2012)
PEDOT:PSS	1.56	0.30	40	Tong *et al.,* (2009**)**
TiO_2	151	0.27		Borgese et al., (2012)
$CH_3NH_3SnI_3$	18.2	0.28	340	Feng (2014**),** Docampo et al., (2013)
$CH_3NH_3PbI_3$	12.8	0.33	340	Feng (2014**),** Docampo et al., (2013)
P3HT:PCBM	6.02	0.35	110	Tahk *et al.,* 2009
Al	70	0.33	100	Huerta *et al.,* 2012

3.4 Finite Element Simulation

In this work, finite element models are built using ABAQUS^{TM} finite element analysis software to predict stress distribution and failure mechanisms in planar flexible substrate lead and tin based perovskite solar cells subjected to bending and stretching. A 2-D design of the model is first created. This is then followed by a subdivision of the model into simple small pieces called elements which are connected at nodes. This step is referred to as meshing. Boundary conditions are imposed, after which loads are applied and results obtained.

3.4.1 Geometry Design

A layered 2-D deformable planar shell beam element was chosen to reduce the computational complexity of the problem of 3-D design. Two set of structures: (1) the photoactive lead/tin perovskite and PDMS (2) PDMS/ PET, PEDOT:PSS, photoactive lead/tin perovskite, P3HT:PCBM, TiO_2 and Al layers were modeled. The dimension of the specimens is specified and in each case, these were partitioned into sections corresponding to the thickness of each layer as presented in table 3.1.

The Young's modulus and Poisson ratio of each material was inputted into the software and subsequently assigned to each section. For bending simulation, a three point fixture was designed, with the two outer fixtures as support and the third fixture (in the middle) as the load on the single and multilayer (beam).

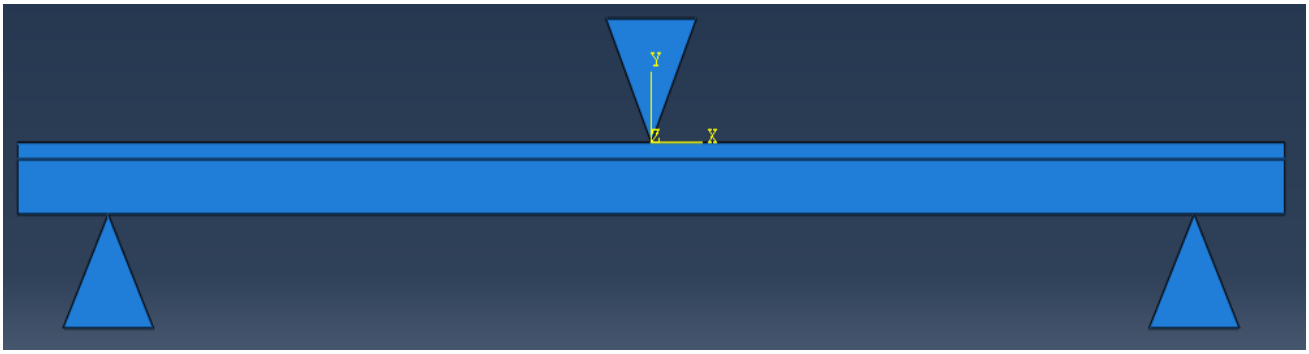

Figure 3.3: Typical 2-D deformable planar lead/tin based perovskite layer on PET under bending.

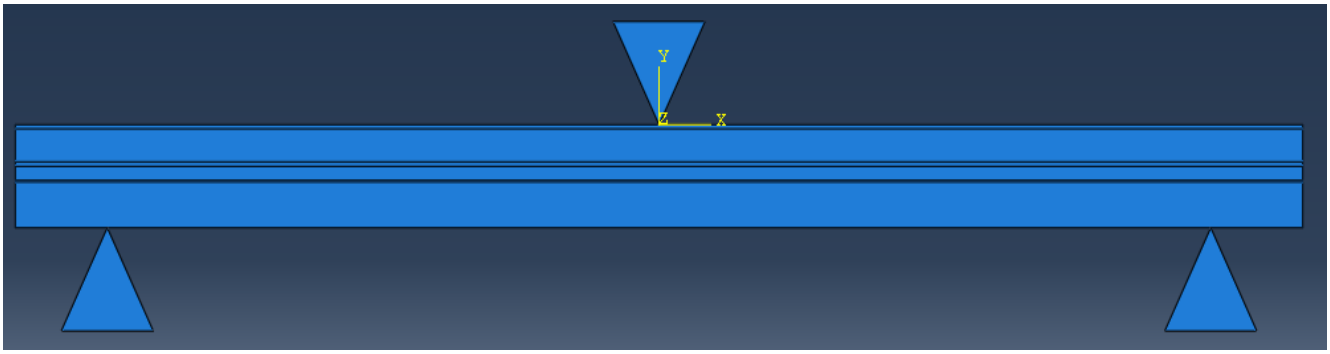

Figure 3.4: Typical 2-D deformable planar multilayered lead/tin based perovskite solar cell geometry under bending.

A buckled structure, which often arises due to factors such as surface roughness of substrate, dust particles or residual stresses was introduced into the model for stretching (figure 3.5 and 3.6). In this research, the buckled structure (wavelength 0.5μm) is assumed to be due to bubble formation during film deposition and this is introduced to make the system more flexible, to observe interfacial failure and to determine energy release rate at the crack tip.

Figure 3.5: Typical 2-D deformable planar lead/tin based perovskite layer on PET under stretching.

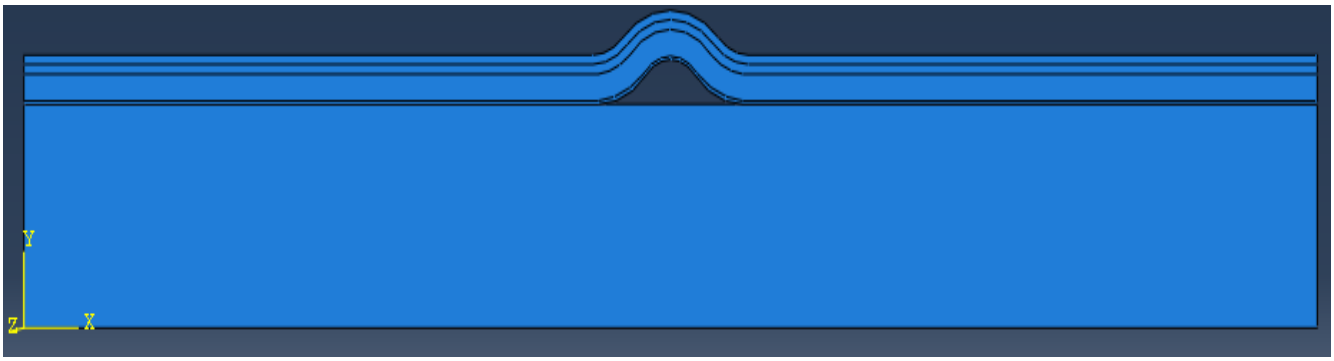

Figure 3.6: Typical 2-D deformable planar multilayered lead/tin based perovskite solar cell geometry under stretching.

3.4.2 Boundary Conditions and Meshing

For bending, boundary conditions were imposed on the multilayers, the roller supports and the fixed holders. These were defined using the displacement/rotation boundary condition to constrain the movement of the selected degrees of freedom to zero and to prescribe the displacement or rotation for each selected degree of freedom. Static loading is applied to the pushdown fixture at the middle of the model with varying loads.

The model was divided into elements for the purpose of meshing. The three point fixtures and the multilayers were suitably meshed independently and convergence was obtained at a mesh size of 100 and 50 elements.

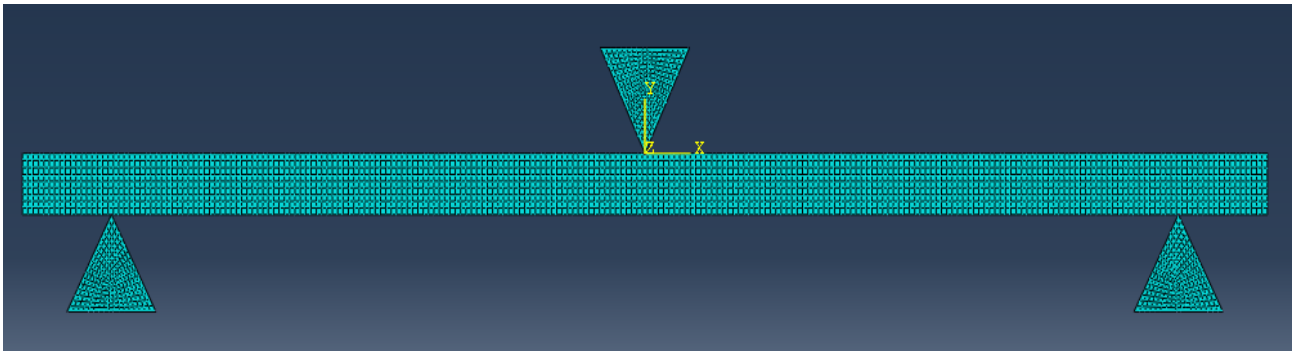

Figure 3.7: Meshed model of lead/tin based perovskite layer on PET under bending.

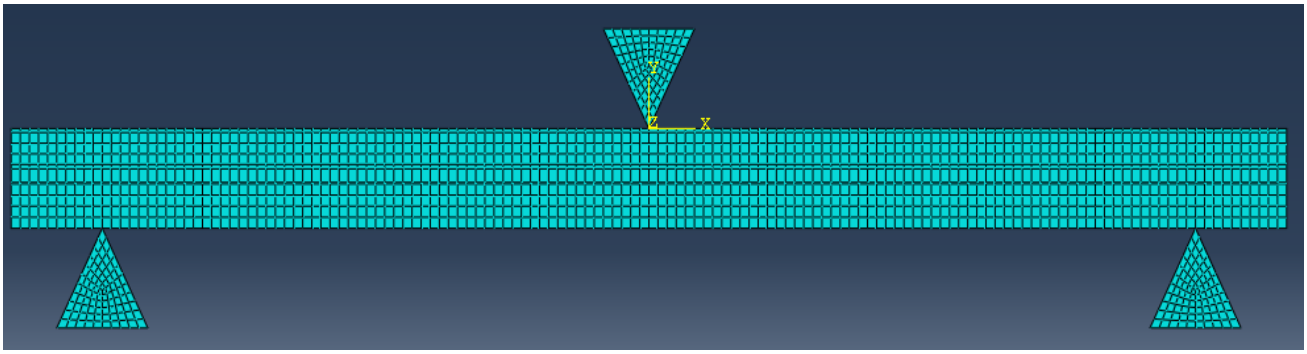

Figure 3.8: Meshed model of multilayered lead/tin based perovskite solar cell under bending.

For models under stretching, structured-quad mesh control was applied so as to control the mesh quality at the defined cracks tips and buckled structure. Displacement/rotation along the y and z-axis was restricted for the substrate, while the interface between the film and substrate was constrained along the y-axis. A master-slave interaction was also imposed on the buckled structure and the surface of the substrate and a tensile loading of 2.5 Mpa applied to both ends of the model.

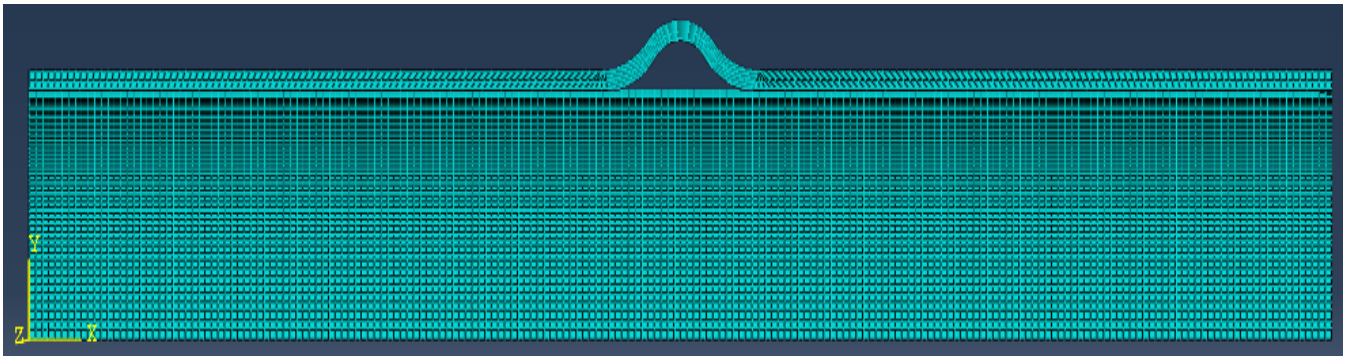

Figure 3.9: Meshed model of lead/tin based perovskite layer on PET under stretching.

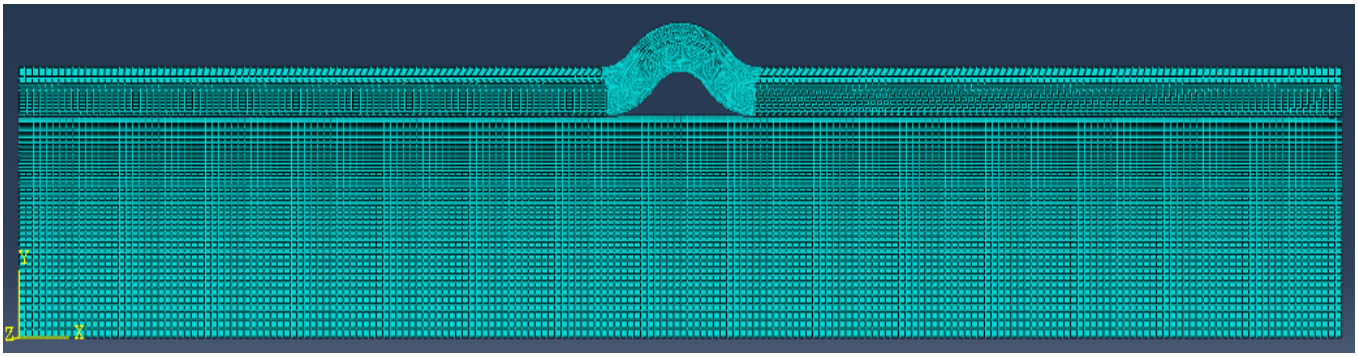

Figure 3.10: Meshed model of multilayered lead/tin based perovskite solar cell under stretching.

3.4.3 Result Visualisation

The completed models were submitted and the deformed shape viewed from the “plot” menu. Both the contours as well as the Von-Mises stresses were presented and discussed in chapter four.

4 Chapter Four: Results and Discussion

4.1 Introduction

Since this research effort is a preliminary work towards understanding the mechanical performance of lead based and tin based perovskite solar cell, the results obtained from the initial analysis (appendix 1) showed that the presence of TiO_2 in the multilayers caused the cells (both lead based and tin based) to deform abnormally when stretched. A plausible explanation for this observation is the relatively high Young's modulus of TiO_2 which makes it resist deformation when compared to other layers. In addition, the relative thickness of the TiO_2 layer makes this effect significant. This result further support the need to substitute TiO_2 since it requires high temperature to anneal and this can destroy flexible substrates.

Another important preliminary observation made was the suitability of PET as substrate for bending and PDMS for stretching. This is also due to the low Young's modulus of PDMS, as it experience deformation on the aluminium fixed holders under bending. PET on the other hand experiences high stresses around the buckled structure when subjected to stretching due to its reduced stretchability. PET can however withstand more strain when subjected to bending.

4.2 Effects of Stretching

4.2.1 Stress Analysis

The full contours of the models are presented in appendix A. The extracts presented in figures 4.1, 4.2, 4.3 and 4.4 shows stress distribution in lead and tin based single layer, and lead and tin based multilayers respectively when subjected to stretching.

The stress distribution has a bell shape across the substrate of the single layer lead based model while that of the tin based model is uniform with no observable shape. High stress locations were observed in the middle section of the buckled structure of the single layers (figures. 4.1 and 4.2).

It can be seen from the modeling results that stress distribution across the tin-based single layer is significantly higher when compared to the corresponding lead-based. For instance, stresses around the defined cracks (both ends of the buckled structure) range between 1.3 – 2.3 GPa for tin-based single layer while the range for lead based is between 301 MPa to 1.9 GPa. Towards the edges of the layers (away from the buckled structure), the stress on the tin based layer is as

high as 3.7 GPa while a much lower stress value of about 2.5 GPa is observed for the lead based single layer. The implication of this observation is that the lead based perovskite material boast of better flexibility under stretching than the tin-based.

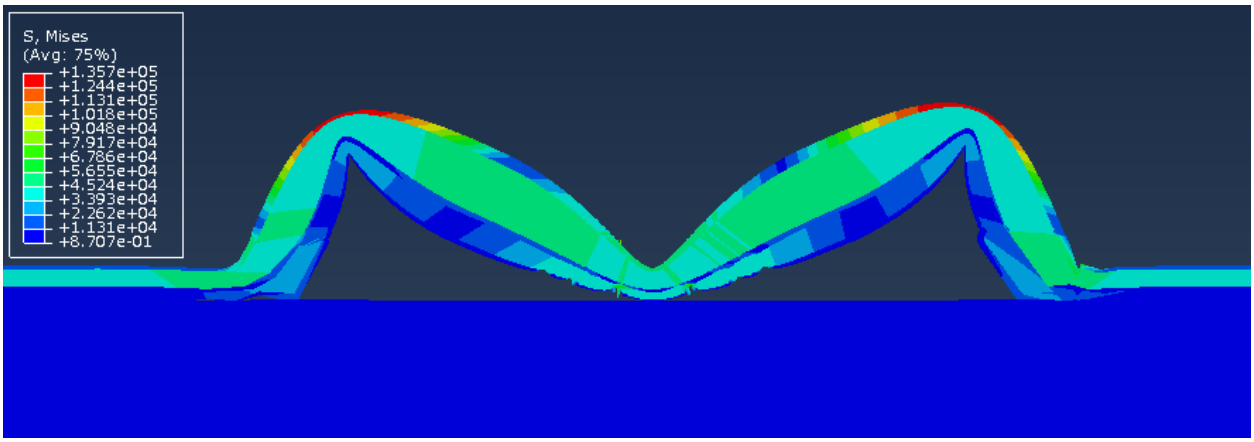

Figure 4.1: Contour extract of multilayer tin-based perovskite containing TiO2 under stretching.

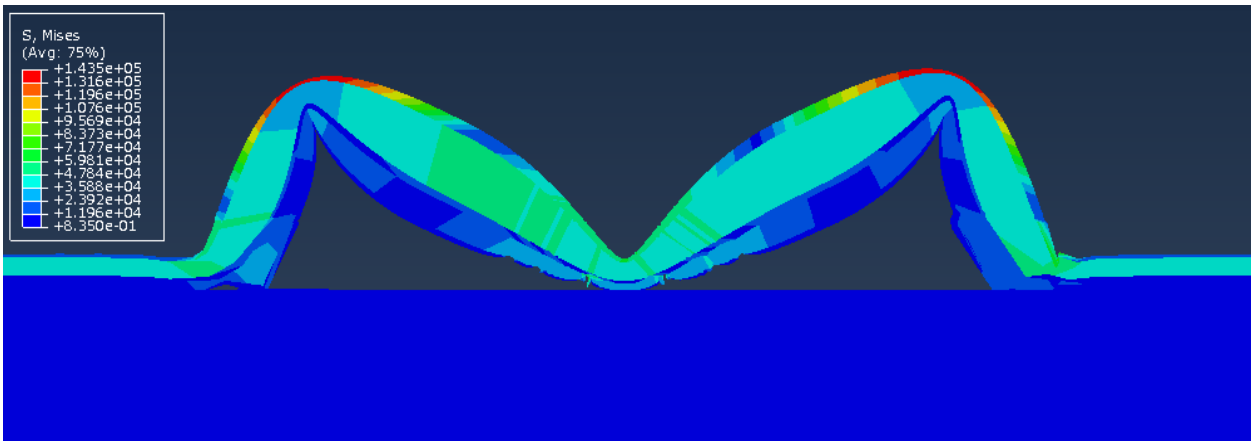

Figure 4.2: Contour extract of multilayer lead-based perovskite containing TiO2 under stretching

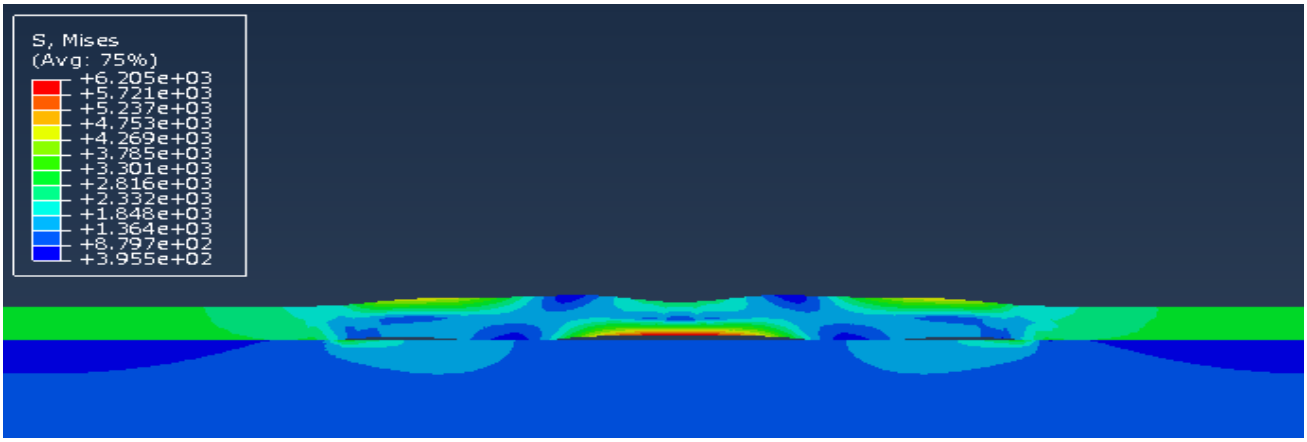

Figure 4.3: Contour extract of MASnI3 on PET under stretching.

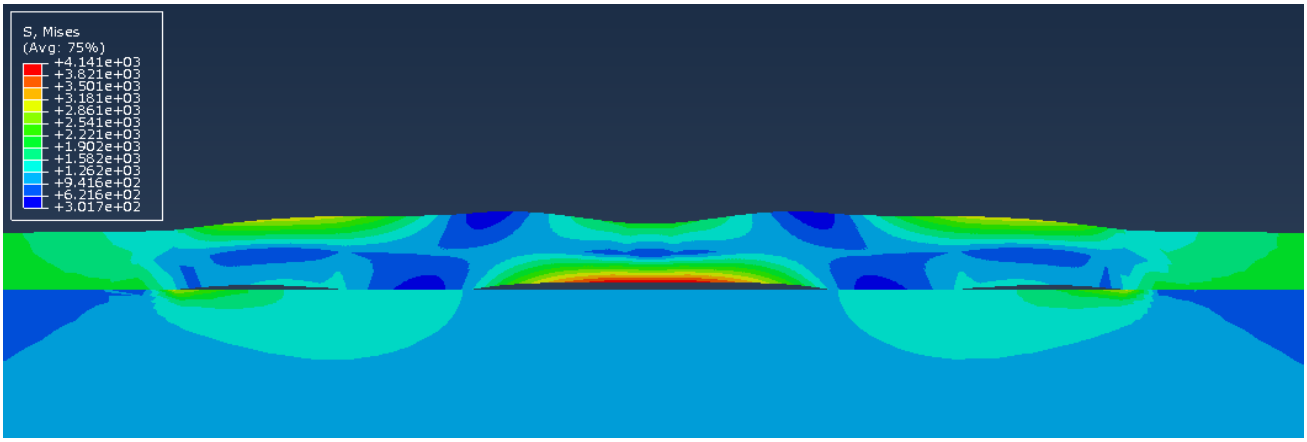

Figure 4.4: Contour extract of MAPbI3 on PET under stretching.

Under similar loadings, interesting stress distribution pattern was observed in the multilayers. Stresses on the aluminium contact layer of the structures are much higher than that at other layers; this is due to the huge difference in elasticity between aluminium and the organic and organic-inorganic materials. Stress values as high as 16 GPa was observed in the aluminum layer suggesting that failure is likely to initiate in this layer.

Contours obtained suggest that the stresses on the aluminium contact decreases and then increases as the buckled structure is approached. This however decreases to a minimum at the center of the buckle. Stress region in the photoactive perovskite material also showed this

pattern with an extended region of relatively high stress observed in the tin based model. A significant difference was observed in the shape of the stress distribution in the PET substrate around the buckled region of the tin and lead based with the latter appearing steeper than the former.

As expected, stress levels in organic layers of PEDOT:PSS and P3HT:PCBM in both model (figure 4.5 and 4.6) were at minimum. However, just as observed in the models for single layers, relatively higher stresses was observed in all the materials of tin based multilayer. This implies that lead based multilayer may be more suitable for applications where stretchability is desirable.

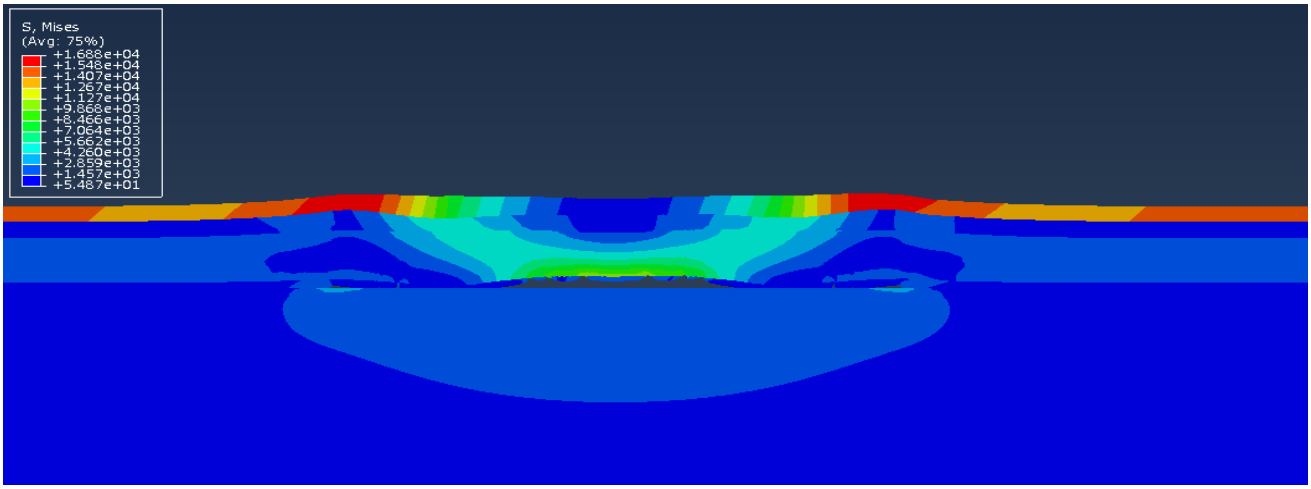

Figure 4.5: Contour extract of multilayer lead-based perovskite solar cell under stretching.

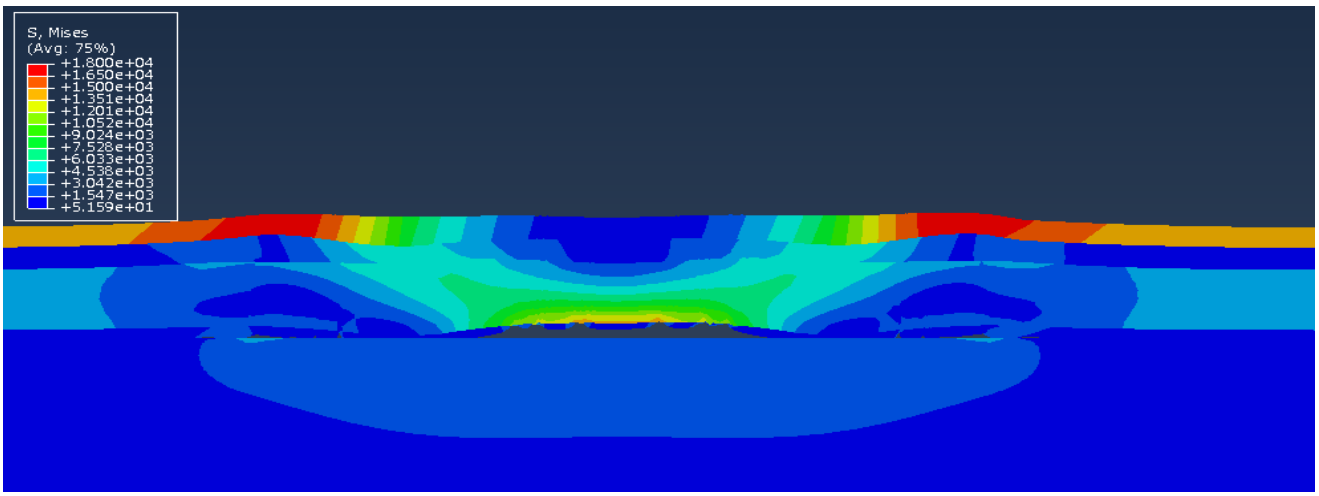

Figure 4.6: Contour extract of multilayer tin-based perovskite solar cell under stretching.

4.2.2 Failure Mechanism

The buckled region of the PEDOT:PSS layer was observed to fail. Although the thickness of the layer is small and may be responsible for the failure, the film material has more effect on the maximum stress than the thickness of the thin film.

The defined cracks were observed to grow slowly towards the edges in all the simulations done. However, no observable interfacial failure was seen among the layers

4.3 Effect of Bending

4.3.1 Stress Analysis

Figures 4.7, 4.8, 4.9 and 4.10 shows the contours of models subjected to bending. As can be seen from the legend, stress levels experienced by models under bending are comparatively lower than those of their analogue under stretching. A comparison of lead and tin based perovskite on PET (figures 4.7 and 4.8) showed a similar stress distribution pattern with the region of high stress observed at the point where the load is applied. Stress level of about 900 MPa was observed at the base of the substrate for both figures.

The results obtained for the multilayers (figures 4.9 and 4.10) did not raise intriguing questions and the stress distribution values were quite low with the exception of the aluminium layer. The high stress region observed in the aluminium layer is the point where the effect of the load applied is felt most.

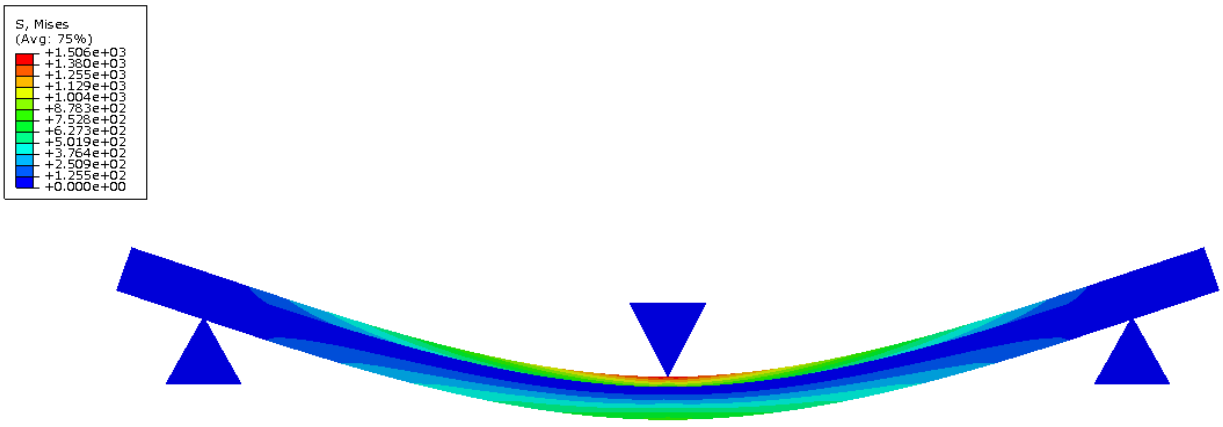

Figure 4.7: Contour plot of MASnI3 on PET under bending.

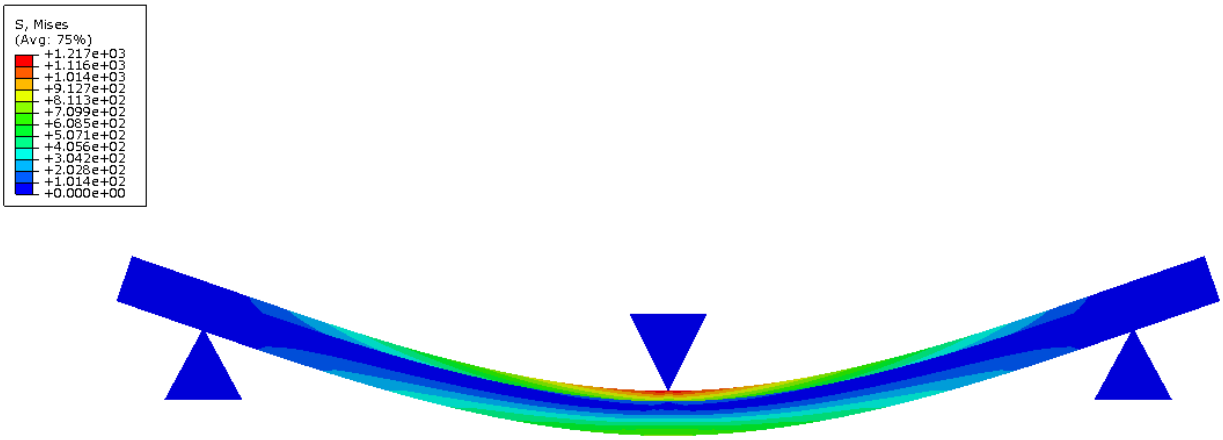

Figure 4.8: Contour plot of MAPbI3 on PET under bending.

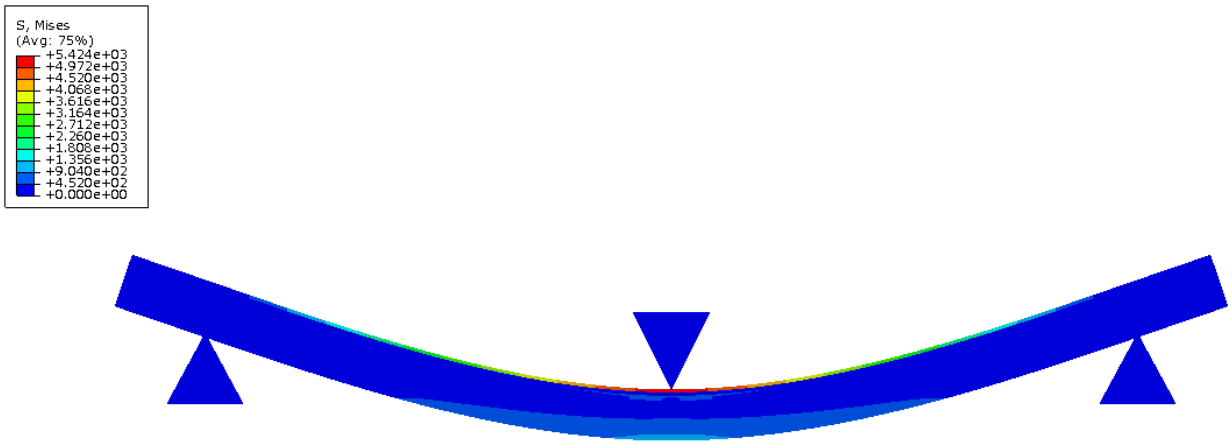

Figure 4.9: Contour plot of multilayer tin-based perovskite solar cell under bending.

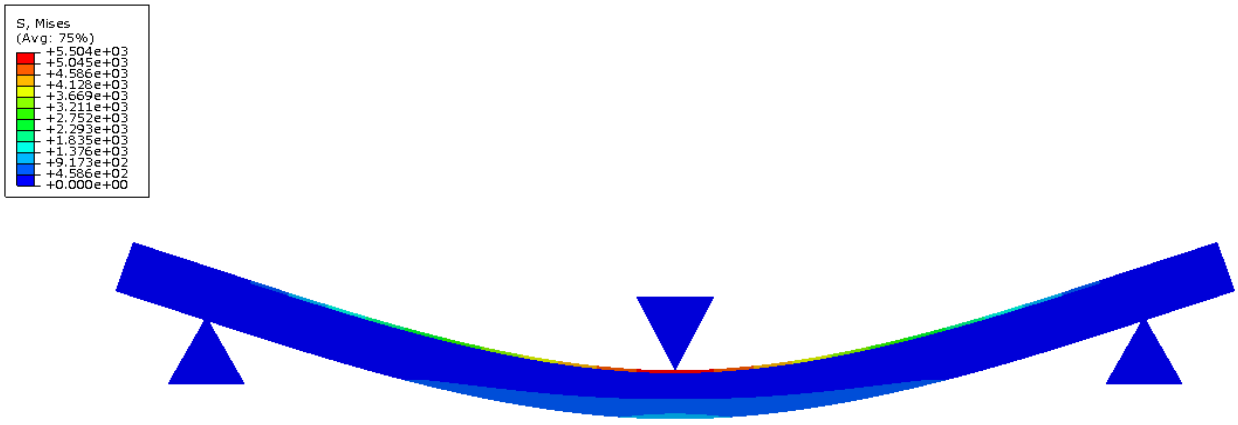

Figure 4.10: Contour plot of multilayer tin-based perovskite solar cell under bending.

4.3.2 Failure Mechanism

The bending results were not very encouraging as no significant failure mode was observed both in the single and multilayers. A possible explanation for these results may be due limited understanding of the mechanics behind bending as it relates to the ABAQUS^{TM} FEA software.

These findings are open for much scrutiny, but some immediate dependable conclusions that can be drawn from it is the suitability of PET as a compliant substrate and the compatibility of PEDOT:PSS and PCBM:P3HT for bending applications.

5 Chapter Five: Conclusion and Recommendations

5.1 Conclusion

Increasing demand for solar cells with competitive efficiencies and wearable performance has continued to drive research and innovation in perovskite based solar cells. In this study, we have successfully demonstrated the need to eliminate the use of TiO_2 nanocrystals which acts only as scaffold for light harvesting as contour obtained showed that its modulus and thickness reduces the mechanical performance of the solar cells where flexibility is needed.

Results obtained from analysis have also shown that both lead and tin based photoactive perovskite material are compatible with flexible substrate as against the widely used rigid glass substrate. However there is a need to employ a more suitable and complaint substrate for application where both flexibility and bendability are desirable.

5.2 Recommendations

A number of possible future studies have been thrown up by this research effort. It is recommended that experimental work be undertaken to verify the result obtained from the simulations done.

Another possible area of future research would be to investigate the mechanical performance of mixed halide and the suitability of other compliant substrate. It would be interesting to assess the effects of and interaction between multiple buckle structures in future research effort.

Further investigation and experimentation into cracks and failure mechanisms not covered in this research is strongly recommended in future work.

6 References

Akogwu, O., Kwabi, D., Midturi, S., Eleruja, M., et al. (2010) Large strain deformation and cracking of nano-scale gold films on PDMS substrate. *Materials Science and Engineering: B*. 170 (1-3), 32–40.

Arkhipov, V.I. & Bässle, H. (2004) Exciton dissociation and charge photogeneration in pristine and doped conjugated polymers. *Phys. Status Solidi A*. 2011152–1187.

Barrows, A., Pearson, A., Kwak, C., Dunbar, A., et al. (2014) Efficient planar heterojunction mixed-halide perovskite solar cells deposited via spray-deposition. *Energy & Environmental Science*. 001–7.

Borgese, L., Gel, M., Bontempi, E., Goudeau, P., et al. (2012) *Surface & Coatings Technology Young modulus and Poisson ratio measurements of TiO 2 thin fi lms deposited with Atomic Layer Deposition*. 2062459–2463.

Brivio, F., Walker, A.B. & Walsh, A. (2013) Structural and electronic properties of hybrid perovskites for high-efficiency thin-film photovoltaics from first-principles. *APL Materials*. 1 (4), 042111.

Burschka, J., Pellet, N., Moon, S.-J., Humphry-Baker, R., et al. (2013) Sequential deposition as a route to high-performance perovskite-sensitized solar cells. *Nature*. 499 (7458), 316–319.

Campbell, W.M., Jolley, K.W., Wagner, P., Wagner, K., et al. (2007) *Highly Efficient Porphyrin Sensitizers for Dye-Sensitized Solar Cells*. 36 (3), 11760–11762.

Chen, L.J., Song, Q.L., Xiong, Z.H., Huang, J.H., et al. (2011) Environment-friendly energy from all-carbon solar cells based on fullerene-C60. *Solar Energy Materials and Solar Cells*. 9 (4), 1138–1140.

Choi, J.J., Yang, X., Norman, Z.M., Billinge, S.J.L., et al. (2014) Structure of methylammonium lead iodide within mesoporous titanium dioxide: active material in high-performance perovskite solar cells. *Nano letters*. 14 (1), 127–133.

Deschler, F., Price, M., Pathak, S., Klintberg, L.E., et al. (2014) High Photoluminescence E ffi ciency and Optically Pumped Lasing in Solution-Processed Mixed Halide Perovskite Semiconductors. *Journal of Physical Chemistry Letters*. 5 (8), 1421–1426.

Docampo, P., Ball, J.M., Darwich, M., Eperon, G.E., et al. (2013) Efficient organometal trihalide perovskite planar-heterojunction solar cells on flexible polymer substrates. *Nature communications*. 42761.

Docampo, P., Guldin, S., Leijtens, T., Noel, N.K., et al. (2014) Lessons learned: from dye-sensitized solar cells to all-solid-state hybrid devices. *Advanced materials (Deerfield Beach, Fla.)*. 26 (24), 4013–4030.

Edri, E., Kirmayer, S., Henning, A., Mukhopadhyay, S., et al. (2014) Why lead methylammonium

tri-iodide perovskite-based solar cells require a mesoporous electron transporting scaffold (but not necessarily a hole conductor). *Nano letters*. 14 (2), 1000–1004.

Edri, E., Kirmayer, S., Mukhopadhyay, S., Gartsman, K., et al. (2014) Elucidating the charge carrier separation and working mechanism of CH3NH3PbI(3-x)Cl(x) perovskite solar cells. *Nature communications*. 53461.

Feng, J. (2014) Mechanical properties of hybrid organic-inorganic CH3NH3BX3 (B = Sn, Pb; X = Br, I) perovskites for solar cell absorbers. *Apl Materials*. 2 (8), 081801.

Grätzel, M. (2003) Dye-sensitized solar cells. *Journal of Photochemistry and Photobiology*. 4145–153.

Green, M. a., Ho-Baillie, A. & Snaith, H.J. (2014) The emergence of perovskite solar cells. *Nature Photonics*. 8 (7), 506–514.

Hao, F., Stoumpos, C.C., Cao, D.H., Chang, R.P.H., et al. (2014) Lead-free solid-state organic–inorganic halide perovskite solar cells. *Nature Photonics*. 8 (6), 489–494.

Hardin, B.E., Snaith, H.J. & McGehee, M.D. (2012) The renaissance of dye-sensitized solar cells. *Nature Photonics*. 6 (3), 162–169.

Heo, J.H., Im, S.H., Noh, J.H., Mandal, T.N., et al. (2013) Efficient Inorganic-organic hybrid heterojunction solar cells containing perovskite compound and polymeric hole conductors. *Nature Photonics*. 7 (June), 486–491.

Hsu, C.-L., Lin, C.-T., Huang, J.-H., Chu, C.-W., et al. (2012) Layer-by-Layer Graphene/TCNQ Stacked Films as Conducting Anodes for Organic Solar Cells. *Acs Nano*. 6 (6), 5031–5039.

Huerta, E., Oliva, A.I., Avilés, F., González-Hernández, J., et al. (2012) Elastic modulus determination of Al-Cu film alloys prepared by thermal diffusion. *Journal of Nanomaterials*. 2012.

Hug, H., Bader, M., Mair, P. & Glatzel, T. (2014) Biophotovoltaics : Natural pigments in dye-sensitized solar cells. *Applied Energy*. 115216–225.

IEA (2011) *End-use sectors*.

Jarlborg, D.T. (1998) Ab-initio calculations of electronic structure and properties of some perovskite oxides : high- T c superconductors and magnetic materials. *Universite de Geneve*

Jeong, H.J., Jeong, H.D., Kim, H.Y., Kim, J.S., et al. (2011) All-Carbon Nanotube-Based Flexible Field-Emission Devices: From Cathode to Anode. *Adv. Funct. Mater*. 211526–1532.

Kalanithi, B. & Rajesh, S. (2014) Mppt Controller Based Solar Tracking System. *IOSR Journal of Mechanical and Civil Engineering*. 78–83.

Kaltenbrunner, M., White, M.S., Głowacki, E.D., Sekitani, T., et al. (2012) Ultrathin and

lightweight organic solar cells with high flexibility. *Nature communications*. 3770.

Khlyabich, P.P., Burkhart, B., Rudenko, A.E. & Thompson, B.C. (2013) Optimization and simplification of polymer e fullerene solar cells through polymer and active layer design. *Polymer*. 54 (20), 5267–5298.

Kim, B.-J., Kim, D.H., Lee, Y.-Y., Shin, H.-W., et al. (2014) Highly efficient and bending durable perovskite solar cells: toward wearable power source. *Energy Environ. Sci.* 001–6.

Kim, H.-S., Lee, C.-R., Im, J.-H., Lee, K.-B., et al. (2012) Lead iodide perovskite sensitized all-solid-state submicron thin film mesoscopic solar cell with efficiency exceeding 9%. *Scientific reports*. 2591.

Kim, J.H., Williams, S.T., Cho, N., Chueh, C.-C., et al. (2014) Enhanced Environmental Stability of Planar Heterojunction Perovskite Solar Cells Based on Blade-Coating. *Advanced Energy Materials*. 1–6.

Kojima, A., Teshima, K., Shirai, Y. & Miyasaka, T. (2009) Organometal halide perovskites as visible-light sensitizers for photovoltaic cells. *Journal of the American Chemical Society*. 131 (17), 6050–6051.

Kumar, M.H., Dharani, S., Leong, W.L., Boix, P.P., et al. (2014) Lead-Free Halide Perovskite Solar Cells with High Photocurrents Realized Through Vacancy Modulation. *Advanced Materials*. 26 (41), 7122–7127.

Lai, Y.-Y., Cheng, Y.-J. & Hsu, C.-S. (2014) Applications of functional fullerene materials in polymer solar cells. *Energy & Environmental Science*. 71866–1883.

Lang, L., Yang, J.-H., Liu, H.-R., Xiang, H.., et al. (2014) First-principle Study On The Electronic And Optical Properties of Cubic ABX3. *Elsevier*. 378 (3), 290–293.

Lee, M.M., Teuscher, J., Miyasaka, T., Murakami, T.N., et al. (2012) Efficient hybrid solar cells based on meso-superstructured organometal halide perovskites. *Science (New York, N.Y.)*. 338 (6107), 643–647.

Lee, Y. & Lee, Y. (2014) Investigation on Thin Film Stress for Flexible Electronics by Curvature Method. *International Journal of Emerging Technology and Advanced Engineering*. 4 (8), 454–457.

Leijtens, T., Eperon, G.E., Pathak, S., Abate, A., et al. (2013) Overcoming ultraviolet light instability of sensitized TiO_2 with meso-superstructured organometal tri-halide perovskite solar cells. *Nature communications*. 42885.

Lipomi, D.J., Chong, H., Vosgueritchian, M., Mei, J., et al. (2012) Toward mechanically robust and intrinsically stretchable organic solar cells: Evolution of photovoltaic properties with tensile strain. *Solar Energy Materials and Solar Cells*. 107355–365.

Liu, D. & Kelly, T.L. (2013) Perovskite solar cells with a planar heterojunction structure prepared using room-temperature solution processing techniques. *Nature Photonics*. 8 (2), 133–138.

Liu, M., Johnston, M.B. & Snaith, H.J. (2013) Efficient planar heterojunction perovskite solar cells by vapour deposition. *Nature*.501 (7467), 395–398. Available from: doi:10.1038/nature12509 [Accessed: 9 July 2014].

Malinkiewicz, O., Yella, A., Lee, Y.H., Espallargas, G.M., et al. (2013) Perovskite solar cells employing organic charge-transport layers. *Nature Photonics*. 8 (2), 128–132.

Marchioro, A., Teuscher, J., Friedrich, D., Kunst, M., et al. (2014) Unravelling the mechanism of photoinduced charge transfer processes in lead iodide perovskite solar cells. *Nature Photonics*. 8 (3), 250–255.

Mcgehee, M.D. (2009) Nanostructured Organic – Inorganic Hybrid Solar Cells. *MRS Bulletin*. 34 (February), 95–100.

Miles, R.W., Zoppi, G. & Forbes, I. (2007) Inorganic photovoltaic cells. *Materials Today*. 10 (11), 21–27.

Noel, N.K., Stranks, S.D., Abate, A., Wehrenfennig, C., et al. (2014) Environmental Science for photovoltaic applications †. *Energy & Environmental Science*. 73061–3068.

Ondrejkovic, P., Marton, P., Guennou, M., Setter, N., et al. (2013) Piezoelectric properties of twinned ferroelectric perovskites with head-to-head and tail-to-tail domain walls. *Physical Review B*. 88 (2), 024114.

Oyewole, O.K. (2011) *Effects of Stretching on Flexible Organic Electronic Structures*. African University of Science and Technology.

Qin, P., Tanaka, S., Ito, S., Tetreault, N., et al. (2014) Inorganic hole conductor-based lead halide perovskite solar cells with 12.4% conversion efficiency. *Nature communications*. 5 (May), 3834.

R . H. Bube (1998) *Photovoltaic Materials*. Vol 1. London, Imperial College Press.

Ramuz, M.P., Vosgueritchian, M., Wei, P., Wang, C., et al. (2012) Evaluation of Solution-Processable Carbon-Based Electrodes for All-Carbon Solar Cells. *ACS Nano*.6 (11), 10384–10395.

Saga, T. (2010) Advances in crystalline silicon solar cell technology for industrial mass production. *NPG Asia Materials*. 2 (3), 96–102.

Sariciftci, N.S. (1999) Polymeric photovoltaic materials. Current Opinion in Solid State and Materials Science. 4373–378.

Scharber, B.M.C., Mühlbacher, D., Koppe, M., Denk, P., et al. (2006) Design Rules for Donors in Bulk-Heterojunction Solar Cells — Towards 10 % Energy-Conversion Efficiency. *Advanced Materials*.18789–794.

Seetharaman S, M., P, N.K., P, N., Singh, S.P., et al. (2014) Efficient Organic Inorganic Hybrid Perovskite Solar Cells Processed in Air. *Phys. Chem. Chem. Phys.*1624691–24696.

Shauddin, S.M. (2013) Comparison among Various Emerging PV Cells with History, Current Status and Future Challenges. *Energy and Power*. [Online] 3 (6), 91–105.

Sigma-aldrich Co Llc (2014) *Materials for Flexible and Printed Electronics*. 2014th edition. . Milwaukee.

Smith, I.C., Hoke, E.T., Solis-Ibarra, D., McGehee, M.D., et al. (2014) A Layered Hybrid Perovskite Solar-Cell Absorber with Enhanced Moisture Stability. *Angewandte Chemie International Edition*. 126 (42), 11414–11417.

Soboyejo, W. (2003) *Mechanical Properties for Engineered Materials*. Marcel Dekker, Inc.

Stoumpos, C.C., Malliakas, C.D. & Kanatzidis, M.G. (2013) Semiconducting tin and lead iodide perovskites with organic cations: phase transitions, high mobilities, and near-infrared photoluminescent properties. *Inorganic chemistry*.52 (15), 9019–9038.

Tahk, D., Lee, H.H. & Khang, D.-Y. (2009) Elastic moduli of organic electronic materials by the buckling method. *Macromolecules*. 427079–7083.

Tan, Z.-K., Moghaddam, R.S., Lai, M.L., Docampo, P., et al. (2014) Bright light-emitting diodes based on organometal halide perovskite. *Nature Nanotechnology*. (August), 1–6.

Tong, T., Babatope, B., Admassie, S., Meng, J., et al. (2009) Adhesion in organic electronic structures. *Journal of Applied Physics*. 106 (8), 083708.

Tsao, J., Science, B.E., Lewis, N. & Crabtree, G. (2006) *Solar FAQs*. 1–24.

Win, D.T. (2006) The Nuclear Waste Issue – Technical Facts and Philosophical Aspects. *AU Journal of Technology*. 10 (1), 1–10.

Xing, G., Mathews, N., Lim, S.S., Yantara, N., et al. (2014) Low-temperature solution-processed wavelength-tunable perovskites for lasing. *Nature materials*. 13 (May), 476–480.

You, J., Hong, Z., Yang, Y.M., Chen, Q., et al. (2014) Perovskite Solar Cells with High Efficiency and Flexibility. *ACS Nano*. 8 (2), 1674–1680.

Zhang, W. & Tong, P. (2012) Structural, elastic, magnetic and electronic properties of 4d perovskite CaTcO3: a DFT+U investigation. *Journal of physics. Condensed matter : an Institute of Physics journal*. 24 (18), 185401.

7 Appendix A

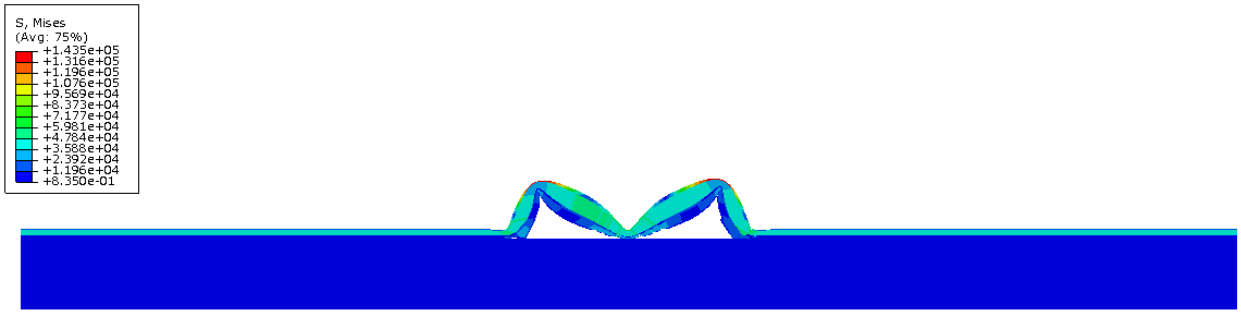

Figure 7.1: Contour plot of multilayer lead-based perovskite containing TiO2 under stretching.

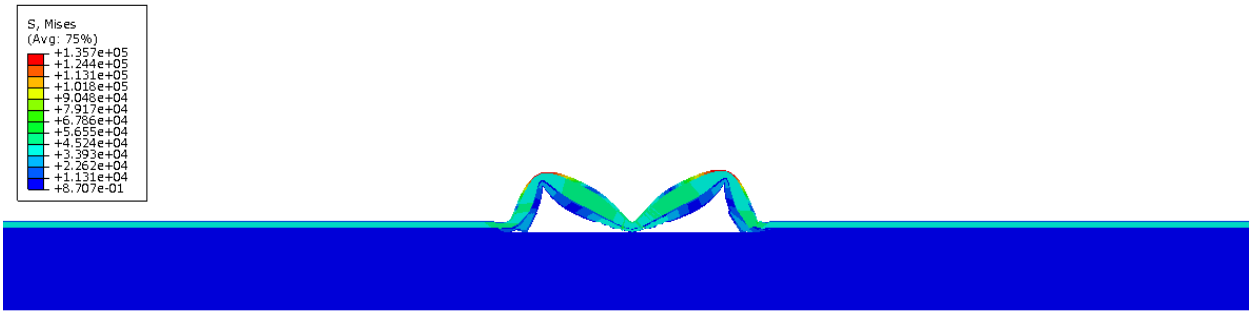

Figure 7.2: Contour plot of multilayer tin-based perovskite containing TiO2 under stretching.

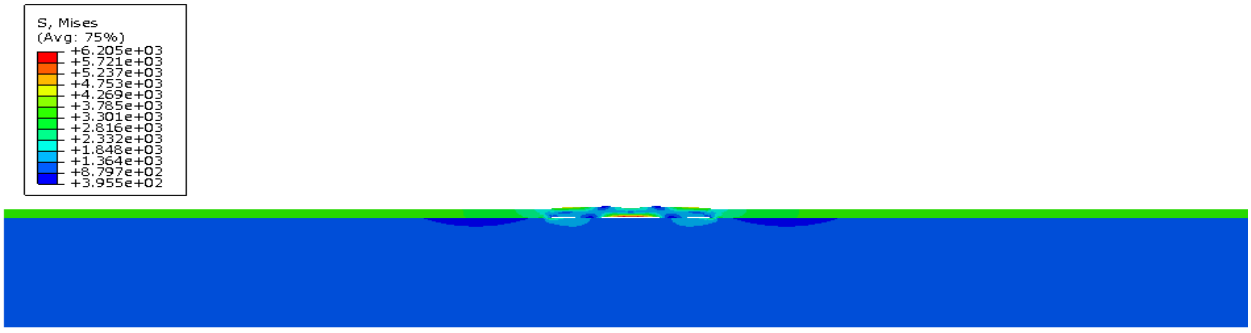

Figure 7.3: Contour plot of MASnI3 on PET under stretching.

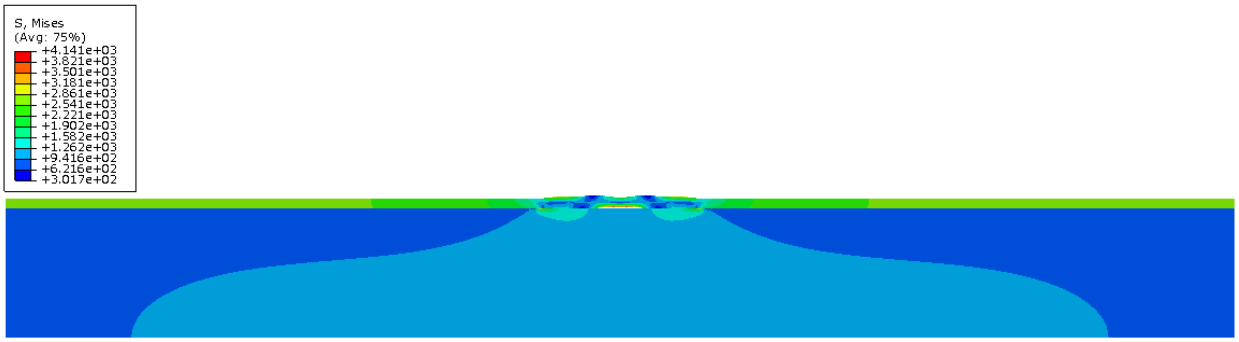

Figure 7.4: Contour plot of MAPbI3 on PET under stretching.

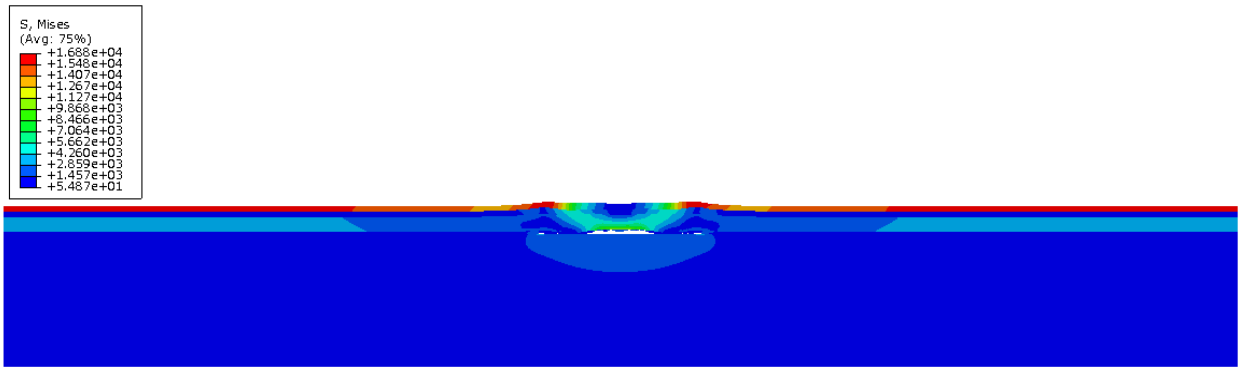

Figure 7.5: Contour plot of multilayer lead-based perovskite solar cell under stretching.

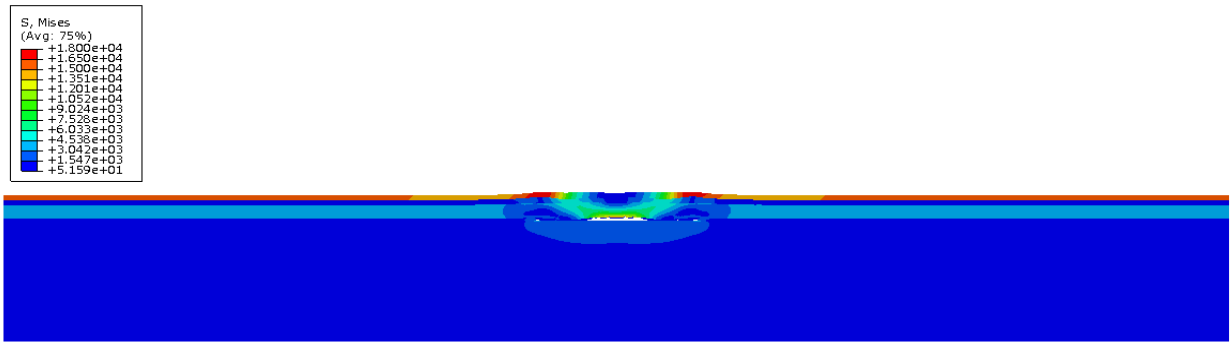

Figure 7.6: Contour plot of multilayer tin-based perovskite solar cell under stretching.